A real-frequency solver for the Anderson impurity model based on bath optimization and cluster perturbation theory

Manuel Zingl[a], Martin Nuss[a], Markus Aichhorn[a]

[a]*Institute of Theoretical and Computational Physics, Graz University of Technology, NAWI Graz, 8010 Graz, Austria*

Abstract

Recently solvers for the Anderson impurity model (AIM) working directly on the real-frequency axis have gained much interest. A simple and yet frequently used impurity solver is exact diagonalization (ED), which is based on a discretization of the AIM bath degrees of freedom. Usually, the bath parameters can not be obtained directly on the real axis, but have to be determined by an ambiguous fit procedure on the Matsubara axis. In this work we present an approach where the bath degrees of freedom of the AIM are first discretized directly on the real-frequency axis using a large number of bath sites (≈ 50). Then, the bath is optimized by unitary transformations such that it separates into two parts that are weakly coupled. One part contains the impurity site, and its interacting Greens functions can be determined by ED. The other larger part is a non-interacting system containing all the remaining bath sites. Finally, the full Green's function of the AIM is calculated via coupling these two parts by cluster perturbation theory.

Keywords: Anderson impurity model, exact diagonalization, cluster perturbation theory, bath optimization

1. Introduction

The single-orbital Anderson impurity model (AIM) [1] can be represented exactly by an interacting site coupled to a bath of infinitely many non-interacting sites. In approaches based on exact diagonalization (ED), the number of sites in the interacting system is restricted, and thus the bath needs to be truncated [2; 3; 4]. This is a delicate step, as there is not an unique procedure. Different ways are used, e.g., fits on the Matsubara axis or continuous fraction expansions [3; 5; 6].

Therefore, various methods improving on ED have been presented in recent years, e.g., the variational exact diagonalization [7], the distributional exact diagonalize [7] and methods based on restricting the basis states [8; 9; 10; 11; 12]. Another way of going beyond ED is the use of cluster perturbation theory (CPT) [13; 14; 15], i.e. the more advanced variational cluster approximation (VCA) [16; 17; 18] as a solver for the AIM [19; 20].

From now on, we assume a single-orbital AIM coupled to a finite, but large bath of $L-1$ non-interacting sites. The basic idea of using CPT as an impurity solver is to separate the L-site AIM into a cluster of size L_C, which includes the impurity site and L_C-1 bath sites, and a non-interacting system consisting of the remaining bath sites. In general, the non-interacting Green's function is specified by the Hamiltonian H^0, that is a matrix in orbital space of size $L \times L$. For illustration purposes (see the sketch in Fig. 1), we denote the upper left $L_C \times L_C$ block in H^0 as the interacting cluster, subsequently H^0_C. The remaining, lower $(L-L_C)\times(L-L_C)$ block describes the remainder of the bath, subsequently H^0_R. The inter-cluster coupling T consists of the two off-diagonal blocks in H_0 connecting H^0_C and H^0_R. The onsite Hubbard interaction on the impurity site (index I) $H_U = U n_{I,\uparrow} n_{I,\downarrow}$ is now added to the cluster Hamiltonian, $H_C = H^0_C + H_U$. There are no interactions in the bath degrees of freedom, hence H^0_R remains unchanged.

In CPT both Hamiltonians (H_C and H^0_R) are solved exactly for their single-particle Green's functions $G_C(\omega)$ and $G_R(\omega)$. Note that $G_R(\omega) = G^0_R(\omega)$, as the remainder of the bath is a non-interacting system. Subsequently the two systems are joined to yield the single-particle Green's function of the full system $G(\omega)$ via the CPT relation [14]

$$G^{-1}(\omega) = \begin{pmatrix} G_C(\omega) & 0 \\ 0 & G_R(\omega) \end{pmatrix}^{-1} - T\,, \tag{1}$$

which is exact in the case of a non-interacting system. In the interacting case, the CPT relation is no longer exact, but a result of perturbation theory in T. CPT approximates the self-energy of the full system by the self-energy of the cluster. To obtain the single-particle Green's function of the interacting cluster, we use the Lanczos procedure [21; 22].

In general, the non-interacting bath can always be transformed to a tridiagonal representation via a Lanczos tridiagonalization, yielding a chain representation of the AIM. This representation straight forwardly allows to define the separation of the interacting cluster and the remainder of bath. However, the situation is not so clear in other representations. Consider for example the case of a star geometry, where all bath sites couple once to the impurity site only. Incorporating just a random set of these star sites into the interacting cluster will lead to a poor discretization of the bath, and hence a poor self-energy.

Any unitary transformation on the non-interacting bath degrees of freedom leaves the physics of the interacting AIM in-

Email address: aichhorn@tugraz.at (Markus Aichhorn)

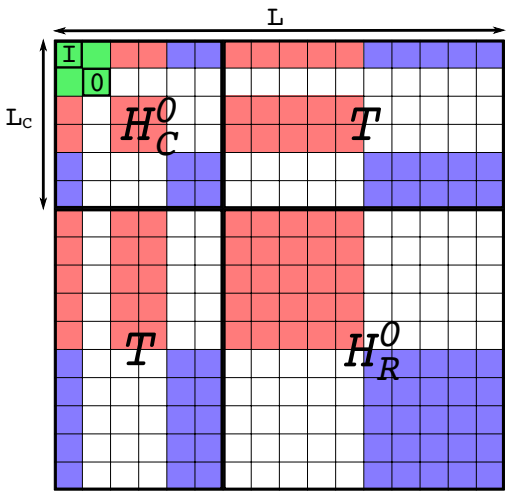

Figure 1: Splitting of the Hamiltonian H^0 into an interacting cluster H_C^0 of $L_C = 6$ sites, the remaining reservoir H_R^0 and the coupling of those two system T. In the specific example of a particle-hole symmetric system the unitary updates are performed in the space of negative energies (red) and equivalently in the space of positive energies (blue). No non-zero matrix elements are generated in the white blocks by the two-dimensional rotation matrices used in this work. The diagonal blocks from top to bottom represent: 1) the impurity, 2) the zero mode inside the cluster, 3) two negative modes inside the cluster, 4) two positive modes inside the cluster, 5) the remaining negative modes in the reservoir and 6) the remaining positive modes in the reservoir.

variant. However, such a transformation will influence the self-energy of the interacting cluster significantly, since it changes the cluster Hamiltonian H_C. Additionally, such transformations will also alter the off-diagonal block T, rendering the resulting perturbation in some cases larger than in others. There exist an infinite number of configurations which all describe the non-interacting bath exactly and which are related via unitary transformations. However, the CPT method itself suggests which baths might be the best: Those which "minimize" the off-diagonal perturbative elements $\|T\|$. The key idea of this work is to use unitary transformations to find those baths with minimal $\|T\|$.

In the following, we outline a way to construct CPT-favorable bath configurations in Sec. 2, and present results in Sec. 3 for a $L = 64$ AIM in semicircular particle-hole symmetric bath.

2. Method

The general form of the non-interacting Hamiltonian for an L-site AIM is

$$H_0 = \epsilon_I c_I^\dagger c_I + \sum_{i=0}^{L-1} \left(t_{iI} c_i^\dagger c_I + \text{h.c.} \right) + \sum_{i<j}^{L-1} \left(t_{ij} c_i^\dagger c_j + \text{h.c.} \right) \quad (2)$$

where the impurity is denoted by the index I and the $L-1$ bath sites by i and j. We omit spin indices, which are summed over, for clarity. To obtain H_0 for an L-site system one can use a star representation, where each bath site couples directly to the impurity site. Then, the parameters of H_0 can be determined by a discretization of the non-interacting bath DOS into equally spaced intervals. Each interval is represented by a delta peak, where the energy positions of the delta peaks correspond to the on-site energies and the hopping parameters are given by the weights of the intervals. Of course, the higher the number of bath sites the better the result of this discretization. In contrast to a fit on the Matsubara axis, which is usually used in ED-like approaches, the discretization on the real axis is a well defined procedure in the sense that it does not rely on the choice of a cost function.

As next step, we perform a unitary transformation R in the bath only with $c_i = R_{i\alpha} d_\alpha$ and $c_i^\dagger = d_\alpha^\dagger R_{\alpha i}^*$, where $RR^\dagger = \mathbb{1}$. The transformed Hamiltonian reads

$$H_0' = \epsilon_I c_I^\dagger c_I + \sum_{\alpha=0}^{L-1} \left(h_{\alpha I} d_\alpha^\dagger c_I + \text{h.c.} \right) + \sum_{\alpha<\beta}^{L-1} \left(h_{\alpha\beta} d_\alpha^\dagger d_\beta + \text{h.c.} \right). \quad (3)$$

The parameters of the Hamiltonian transform like $h_{\alpha I} = \sum_i R_{\alpha i}^* t_{iI}$ and $h_{\alpha\beta} = \sum_{i,j}^{L-1} R_{\alpha i}^* t_{ij} R_{j\beta}$. Such a transformation leaves the impurity state I and consequently ϵ_I invariant.

We define an "energy" of a certain bath configuration via the 2-norm of the off diagonal blocks T

$$E = \frac{1}{N_T} \sum_{i,j}^{L} |T_{ij}|^2 , \quad (4)$$

where the number of elements in T is $N_T = L_C \cdot (L - L_C)$. Transformations on the bath degrees of freedom included in the interacting cluster do not influence the resulting self-energy. The same is true for transformations in the remainder of the bath. This imposes a constraint on the energy E, namely, it has to be invariant with respect to such transformations, which is indeed fulfilled by the 2-norm.

The key idea of this work is now to find an optimal bath configuration for CPT by minimizing the energy functional Eq. (4). Since the configuration space of T_{ij} is high dimensional, we use a Monte Carlo procedure to find configurations with small E. Initially we perform global updates in all dimensions with random rotation matrices to obtain a randomized starting representation of H_0. Then, we move through the space of possible H_0 by proposing random local updates R. In general any unitary update $R = e^{iM}$, with $M = M^\dagger$ would be allowed, but here we restrict ourselves to two-dimensional rotation matrices for the local updates

$$R = \begin{pmatrix} 1 & 0 & \dots & 0 & 0 & \dots & 0 & \dots & 0 \\ 0 & 1 & \dots & 0 & 0 & \dots & 0 & \dots & 0 \\ \dots & \dots & \dots & \dots & \dots & \dots & \dots & \dots & 0 \\ 0 & 0 & \dots & \cos(\phi) & 0 & \dots & -\sin(\phi) & \dots & 0 \\ 0 & 0 & \dots & 0 & 1 & \dots & 0 & \dots & 0 \\ \dots & \dots & \dots & \dots & \dots & \dots & \dots & \dots & 0 \\ 0 & 0 & \dots & \sin(\phi) & 0 & \dots & \cos(\phi) & \dots & 0 \\ \dots & \dots & \dots & \dots & \dots & \dots & \dots & \dots & \dots \\ 0 & 0 & \dots & 0 & 0 & \dots & 0 & \dots & 1 \end{pmatrix}$$

A local update matrix $R(x, y, \phi)$ is drawn by choosing two random integers $x, y \in [1, L-1]$ representing the plane of

rotation and one rotation angle $\phi \in [0, 2\pi[$. A new configuration with energy E' is accepted with probability $p = \min\left(1, e^{-\gamma(E'-E)}\right)$. We use simulated annealing to obtain low energy CPT bath configurations by increasing the parameter γ.

Although bath rotations leave the particle-hole symmetry invariant on the L-site H_0, they destroy it on the L_C-site cluster in the interacting case. Therefore, as shown in Fig. 1, we split the bath sites into an equal amount of positive (blue elements) and negative energy (red elements) sites and one zero mode (green 0). Updates are performed simultaneously on the positive and negative modes which leaves the whole bath, the bath in the cluster as well as the remaining bath particle-hole invariant also if the interaction is turned on. To avoid a Kramers-degenerate ground state for particle-hole symmetric systems, clusters with an even number of sites L_C are chosen. This implies that one bath site (the zero mode) is exactly located at zero energy. Zero mode updates can not be achieved by two dimensional rotations without breaking particle-hole symmetry of the cluster, but would rather require special unitary transformations involving at least three bath sites. For the proof of concept, we refrain from updating the zero mode, i.e. the green elements in Fig. 1 do not change, and note that the zero mode coupling is determined by the initial discretization of the system. Although this restrictes the space of trial bath representations, we leave the zero mode updates for future works.

Next to E as defined in Eq. 4, which reflects the magnitude of the perturbation, we evaluate the influence of the CPT truncation by comparing the non-interacting single-particle impurity Green's function of the full system $G^I_0(\omega)$ to the one considering only the sites in the cluster $G^I_{0,C}(\omega)$. The resulting quantity

$$\chi^2_C = \int d\omega \left| G^I_0(\omega + i\eta) - G^I_{0,C}(\omega + i\eta) \right|^2 , \qquad (5)$$

reflects the ability of the L_c cluster sites to represent the bath degrees of freedom. A-priori a positive correlation of E and χ^2_C is not ensured but expected. We emphazise that χ^2_C is not used in the algorithm, but only serves as a measurement to asses the quality of the bath optimization. To evaluate Eq. 5 we use a numerical broadening of $\eta = 0.02\,\mathrm{eV}$.

3. Results

Here we discuss a single interacting impurity in a particle-hole symmetric semi-circular bath with a half-bandwidth of 1 eV. For the bath optimization we use a discretized system with a total number of $L = 64$ sites and an interacting cluster of $L_C = 10$. The interacting cluster includes the impurity site, one zero mode and five additional positive and negative bath sites each. The discretized DOS is shown in the top graph of Fig. 4 (blue line).

Fig. 2 shows that smaller perturbative elements E correlate positively with smaller χ^2_C, indicating a better representation of the non-interacting bath by the sites contained in the interacting cluster. We compare intermediate bath configurations (black crosses) to the random initial configuration (orange star), a star representation by choosing ten sites at random to enter the interacting cluster (cyan triangle) and the 10-site chain representation (green circle). Note that the chain representation hosts only one perturbative matrix element, which is however large. In all cases one finds a higher χ^2_C with respect to the final result of the optimization (blue cross). Of course, due to the optimization the number of elements in T grows, but their magnitude becomes tiny as compared to the chain or the star representation.

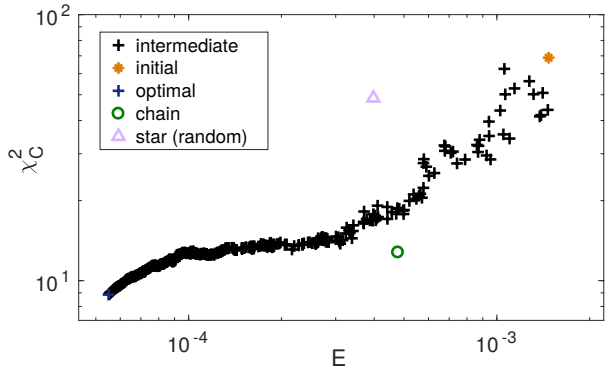

Figure 2: Correlation of the cost function χ^2_C and the Monte Carlo energy E at intermediate steps of the optimization procedure (black crosses). χ^2_C measures the quality of the representation of the non-interacting full system by the cluster only. We show in addition the random starting point (orange star), the optimized representation (blue cross), the respective values of a chain representation cut after 10 sites (green circle) and an arbitrary selected 10-site star (cyan triangle).

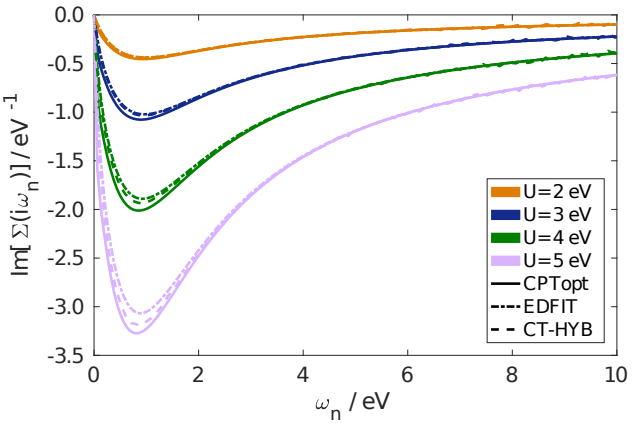

Figure 3: Matsubara self-energy for the AIM with a particle-hole symmetric semi-circular bath DOS. The self-energy of the optimized 10-site cluster (full lines) compared to the ED self-energy of a fitted 10-site system (dash-dotted lines) and a CT-HYB result using the continuous bath DOS (dashed lines). The self-energy is shown for interaction values of $U = 2, 3, 4$ and 5 eV.

To further asses the quality of the optimization scheme we calculate the CPT self-energy of the resulting system on the Matsubara axis for different values of U and compare it to the exact CTHYB result, and to a self-energy obtained with a plain ED calculation for a truncated system with 10 sites (see Fig. 3). The TRIQS library [23] and the TRIQS/CTHYB solver [24] are used to obtain the Matsubara self-energy for the AIM at in inverse temperature of $\beta = 100\,\mathrm{eV}^{-1}$. For the ED calculation we perform a fit of $G_0\,(i\omega)$ on the Matsubara axis to obtain

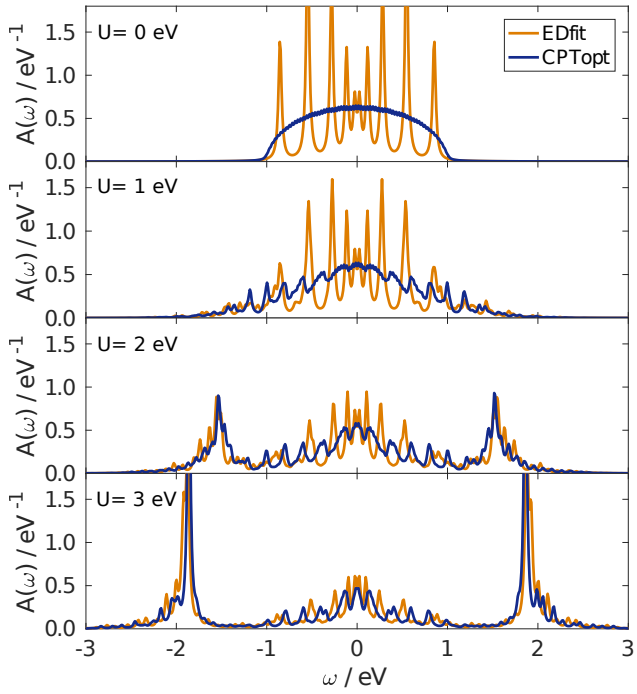

Figure 4: Spectral function $A(\omega)$ of the AIM with a particle-hole symmetric semi-circular bath DOS. The CPT interacting spectral function $A(\omega)$ of the optimized system of size $L = 64$ and $L_C = 10$ (blue) is compared to the ED result for a 10-site system (orange) at interactions $U = 0, 1, 2$ and 3 eV. A numerical broadening of $\eta = 0.02$ eV was used to calculate the spectral function.

the bath parameters of a 10-sites system in chain representation $G^I_{0,ED}(i\omega_n)$ by minimizing the cost function

$$\chi^2_{ED} = \sum_n W_n \left| G^I_0(i\omega_n)^{-1} - G^I_{0,ED}(i\omega_n)^{-1} \right|^2 . \qquad (6)$$

We employ the simplex search method by Lagarias *et al.* [25] and impose particle-hole symmetry to reduce the number of fit parameters. A Matsubara grid with 1024 points at a fictitious temperature corresponding to $\beta = 100\,\mathrm{eV}^{-1}$ is used. The ED solver itself is used at zero-temperature. The cost function Eq. 6 is a heuristic choice and can also take various other forms, e.g. with a different definition of the distance or a different weight W_n [5; 6]. This leads to an ad-hoc determination of the bath parameters and introduces some ambiguity to the solution of the AIM. In this work we set $W_n = 1/\omega_n$.

In Fig. 4 we show the spectral function $A(\omega)$ of the full optimized system ($L = 64$) for interaction values of $U = 0, 1, 2,$ and 3 eV, and compare it to the spectral function of the 10-site ED system. The graph for $U = 0$ eV shows that the CPT result is, up to the influence of the discretization, exact for non-interacting systems. As expected the ED results show strong finite size effects. CPT can improve on the ED result also for finite interaction values.

4. Conclusion

In this work we introduced a bath optimization scheme for the Anderson impurity model. Using unitary transformations in the bath degrees of freedom, we minimize the coupling between a small cluster containing the impurity site with the interactions, and the remaining sites of the bath. These transformations leaves the impurity DOS of the non-interacting bath invariant. In general, the proposed scheme is useful for all CPT-based methods when parts of the entire system are non-interacting, but it does in principle also provide a guideline to construct finite-size representations of hybridization functions as needed, e.g., in the framework of dynamical mean-field theory. For a large enough number of bath sites, the initial AIM can be obtained directly on the real axis, and thus, an ambiguous fit on the Matsubara axis can be avoided. The computational cost of CPT is similar to exact diagonalization (ED). In this work we have presented a proof of concept, but anticipated to explore the bath optimization scheme also for multi-orbital impurity models.

Acknowledgments

The authors acknowledge financial support from the Austrian Science Fund (Y746, P26220, F04103) as well as NAWI Graz.

References

[1] P. W. Anderson, Localized magnetic states in metals, Phys. Rev. 124 (1961) 41–53. doi:10.1103/PhysRev.124.41.

[2] M. Caffarel, W. Krauth, Exact diagonalization approach to correlated fermions in infinite dimensions: Mott transition and superconductivity, Phys. Rev. Lett. 72 (1994) 1545–1548. doi:10.1103/PhysRevLett.72.1545.
URL https://link.aps.org/doi/10.1103/PhysRevLett.72.1545

[3] A. Georges, G. Kotliar, W. Krauth, M. J. Rozenberg, Dynamical mean-field theory of strongly correlated fermion systems and the limit of infinite dimensions, Rev. Mod. Phys. 68 (1996) 13–125. doi:10.1103/RevModPhys.68.13.

[4] M. Capone, L. de' Medici, A. Georges, Solving the dynamical mean-field theory at very low temperatures using the lanczos exact diagonalization, Phys. Rev. B 76 (2007) 245116. doi:10.1103/PhysRevB.76.245116.
URL https://link.aps.org/doi/10.1103/PhysRevB.76.245116

[5] A. Liebsch, H. Ishida, Temperature and bath size in exact diagonalization dynamical mean field theory, J. Phys.: Condens. Matter 24 (5) (2012) 053201. doi:10.1088/0953-8984/24/5/053201.

[6] D. Sénéchal, Bath optimization in the cellular dynamical mean-field theory, Phys. Rev. B 81 (2010) 235125. doi:10.1103/PhysRevB.81.235125.

[7] M. Schüler, C. Renk, T. O. Wehling, Variational exact diagonalization method for anderson impurity models, Phys. Rev. B 91 (2015) 235142. doi:10.1103/PhysRevB.91.235142.

[8] D. Zgid, G. K.-L. Chan, Dynamical mean-field theory from a quantum chemical perspective, The Journal of Chemical Physics 134 (9) (2011) 094115. doi:10.1063/1.3556707.

[9] D. Zgid, E. Gull, G. K.-L. Chan, Truncated configuration interaction expansions as solvers for correlated quantum impurity models and dynamical mean-field theory, Phys. Rev. B 86 (2012) 165128. doi:10.1103/PhysRevB.86.165128.

[10] C. Lin, A. A. Demkov, Efficient variational approach to the impurity problem and its application to the dynamical mean-field theory, Phys. Rev. B 88 (2013) 035123. doi:10.1103/PhysRevB.88.035123.
URL https://link.aps.org/doi/10.1103/PhysRevB.88.035123

[11] Y. Lu, M. Höppner, O. Gunnarsson, M. W. Haverkort, Efficient real-frequency solver for dynamical mean-field theory, Phys. Rev. B 90 (2014) 085102. doi:10.1103/PhysRevB.90.085102.

[12] A. Go, A. J. Millis, arxiv.org:1703.04928.
[13] C. Gros, R. Valentí, Cluster expansion for the self-energy: A simple many-body method for interpreting the photoemission spectra of correlated fermi systems, Phys. Rev. B 48 (1993) 418–425. doi:10.1103/PhysRevB.48.418.
[14] D. Sénéchal, D. Perez, M. Pioro-Ladrière, Spectral weight of the hubbard model through cluster perturbation theory, Phys. Rev. Lett. 84 (2000) 522–525. doi:10.1103/PhysRevLett.84.522.
[15] D. Sénéchal, D. Perez, D. Plouffe, Cluster perturbation theory for Hubbard models, Phys. Rev. B 66 (2002) 075129. doi:10.1103/PhysRevB.66.075129.
[16] M. Potthoff, M. Aichhorn, C. Dahnken, Variational cluster approach to correlated electron systems in low dimensions, Phys. Rev. Lett. 91 (2003) 206402. doi:10.1103/PhysRevLett.91.206402.
[17] Potthoff, M., Self-energy-functional approach to systems of correlated electronsdoi:10.1140/epjb/e2003-00121-8.
[18] Potthoff, M., Self-energy-functional approach: Analytical results and the mott-hubbard transition, Eur. Phys. J. B 36 (3) (2003) 335–348. doi:10.1140/epjb/e2003-00352-7.
[19] M. Nuss, E. Arrigoni, M. Aichhorn, W. von der Linden, Variational cluster approach to the single-impurity anderson model, Phys. Rev. B 85 (2012) 235107. doi:10.1103/PhysRevB.85.235107.
[20] C. Weber, A. Amaricci, M. Capone, P. B. Littlewood, Augmented hybrid exact-diagonalization solver for dynamical mean field theory, Phys. Rev. B 86 (2012) 115136. doi:10.1103/PhysRevB.86.115136.
[21] C. Lanczos, An iteration method for the solution of the eigenvalue problem of linear differential and integral operators, J. Res. Natl. Stand. 45 (1950) 255–282.
[22] A. Ruhe, Implementation aspects of band Lanczos algorithms for computation of eigenvalues of large sparse symmetric matrices, Math. Comp. 33 (1979) 680–687. doi:10.1090/S0025-5718-1979-0521282-9.
[23] Triqs: A toolbox for research on interacting quantum systems, Comput. Phys. Commun. 196 (2015) 398 – 415. doi:http://dx.doi.org/10.1016/j.cpc.2015.04.023.
[24] P. Seth, I. Krivenko, M. Ferrero, O. Parcollet, Triqs/cthyb: A continuous-time quantum monte carlo hybridisation expansion solver for quantum impurity problems, Comput. Phys. Commun. 200 (2016) 274 – 284. doi:https://doi.org/10.1016/j.cpc.2015.10.023.
[25] J. C. Lagarias, J. A. Reeds, M. H. Wright, P. E. Wright, Convergence properties of the nelder–mead simplex method in low dimensions, SIAM Journal on Optimization 9 (1) (1998) 112–147. doi:10.1137/S1052623496303470.